Chapter 3
Braking Control Systems Design: Actuators with Continuous Dynamics

3.1 Introduction

This chapter addresses the problem of braking control design based on actuators with continuous dynamics (see Section 1.3 for their dynamic description).

Of course, the actuator performance forces the engineer to design the braking control system accordingly. Here, for the case of an actuator with continuous dynamics we show how to design a wheel slip controller that can guarantee closed-loop stability and acceptable performance in all possible working conditions by solving a regulation problem. It will be also clear that, because the braking controller is a safety-oriented aid for the driver, it must be switched on and off according to the current manoeuvre. Thus, an appropriate activation and deactivation logic must be designed to accomplish this task.

Further, we investigate the wheel slip control problem starting from a double-corner model, *i.e.*, taking into account the load transfer phenomena. The analysis highlights the effects of dynamic coupling between front and rear axles and its impact on ABS systems design. This leads to the selection of an alternative controlled variable for the braking control of the rear wheel, which arises from the idea of interlocking the rear wheels with the front wheels to achieve a more favorable dynamic behaviour while maintaining a SISO approach to wheel slip control design.

3.2 Wheel Slip Control

In braking control systems, two output variables are usually considered for regulation purposes: wheel deceleration and wheel slip. The traditional controlled variable, which is still used in some ABS systems, is the wheel deceleration. This is due to the fact that it can be easily measured with a simple

wheel encoder (see Appendix B for a discussion on this topic). However, it can be dynamically critical if the road surface changes rapidly. On the other hand, the regulation of the wheel slip is very robust from the dynamical point of view, but the slip measurement is critical, since it requires the estimation of the speed of the vehicle (see Chapter 5 for more details on this issue). Noise sensitivity of slip control hence is a critical issue, especially at low speed.

Thus, the aim of this section is to analyse the merits and drawbacks of slip and deceleration control when both are set up as regulation problems. Further, having made it clear that wheel slip control is the most suitable choice for the design of braking controllers that are robust with respect to road surface variations, the design steps for the synthesis of a linear wheel slip controller will be presented and discussed.

To do this, we will adopt a frequency-domain approach, and start by studying the control problem considering the braking dynamics described by the single-corner model.

Within this context, and based on the analysis performed in Section 2.5.1, the regulation of the wheel slip has a straightforward graphical interpretation in the (λ, η) domain, as displayed in Figure 3.1, where the equilibrium manifold $\eta(\lambda)$ given in (2.34) is depicted in four different road conditions.

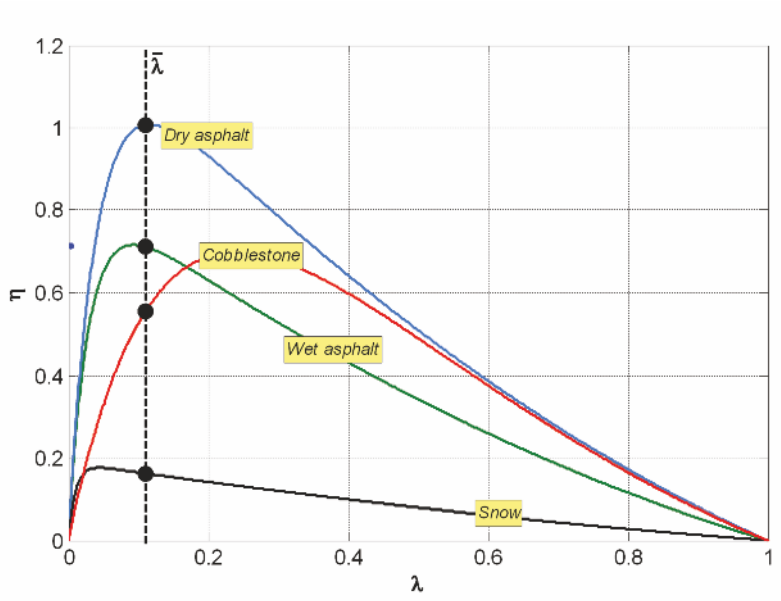

Figure 3.1 Graphical interpretation of slip control in the (λ, η) domain. The *vertical dashed line* represents the set-point $\overline{\lambda}$. The *dots* represent the equilibrium points, for different road conditions

Note that, whatever the value of $\overline{\lambda}$ ($0 \leq \overline{\lambda} \leq 1$), this regulation scheme guarantees the uniqueness of the equilibrium point.

Now, let us consider the transfer function model $G_\lambda(s)$ given in Equation 2.46, in a unitary negative feedback closed-loop with the simplest controller form, *i.e.*, a proportional controller with constant gain K. The closed-loop system is shown in Figure 3.2.

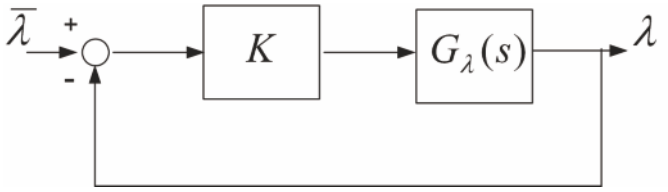

Figure 3.2 Wheel slip closed-loop system with a proportional controller

To analyse the dynamic properties of the slip control system, let us compute the characteristic polynomial $\chi_\lambda(s)$ of the closed-loop system, which, in view of the negative feedback, is given by

$$\chi_\lambda(s) = s + \frac{1}{\overline{v}} \left[\frac{\mu_1(\overline{\lambda}) F_z}{m} \left((1 - \overline{\lambda}) + \frac{mr^2}{J} \right) + K \frac{r}{J} \right].$$

Accordingly, the following stability condition can be derived (note that it does not depend on $\overline{v}$).

Stability Condition for Slip Control
The closed-loop stability condition for the slip control system shown in Figure 3.2 is given by

$$K > -\frac{\mu_1(\overline{\lambda}) F_z \, J}{m \, r} \left((1 - \overline{\lambda}) + \frac{mr^2}{J} \right). \tag{3.1}$$

This condition obviously always holds when $\mu_1(\overline{\lambda}) > 0$. However, also when $\mu_1(\overline{\lambda}) < 0$, since $|\mu_1(\overline{\lambda})|$ is bounded, it is always possible to find a value $\overline{K}$ such that for $K > \overline{K}$, the closed-loop system in Figure 3.2 is asymptotically stable in every working condition, namely for every value of $\overline{\lambda}$ and for every road condition (note from Figure 3.1 that, *e.g.*, on snow/icy roads, $\overline{\lambda} = 0.09$ corresponds to an open-loop unstable equilibrium, since $\mu_1(\overline{\lambda}) < 0$, but the closed-loop stability can be guaranteed).

Note that condition (3.1) has also an intuitive geometrical interpretation. To see this, note that the condition $K > \overline{K}$ can be graphically identified by first intersecting equilibrium manifold in the (λ, η) plane (see Figure 3.1) with the line of negative slope $\overline{K}$ cutting the λ axis in $\overline{\lambda}$. Note also that in doing so, the intersection between the equilibrium manifold in the (λ, η) plane

determines the actual equilibrium value of the wheel slip, say $\tilde{\lambda}_f$, which (as we are using a proportional controller) is in general different from the set-point value $\overline{\lambda}$. If K satisfies the bound in (3.1) for all values of $\overline{\lambda}$ and for all road conditions, then the closed-loop equilibrium is unique and it is locally asymptotically stable.

The performed analysis illustrates why slip control is an attractive approach in braking control systems:

- Given a set-point $\overline{\lambda}$, it guarantees the uniqueness of the equilibrium.
- The choice of $\overline{\lambda}$ is not critical; as a matter of fact, it is easy to find a value of $\overline{\lambda}$ (*e.g.*, $\overline{\lambda} = 0.09$, see Figure 3.1) that provides very good results (even if slightly sub-optimal) for every road condition. This feature is very appealing since it allows the use of a fixed structure controller, with no need for online identification and detection of the road conditions.
- With a fixed structure controller (*i.e.*, a fixed value of K), the asymptotic stability of the closed-loop is guaranteed for every value of $\overline{\lambda}$ and for every road condition.

The major flaw of slip control is that the measurement of the wheel slip is comparatively difficult and unreliable, especially at low speed. Hence, the sensitivity of wheel slip control to measurement errors is a key issue. Chapter 6 provides a control strategy able of alleviating the problems related to this issue.

3.3 Wheel Deceleration Control

If the controlled variable is the normalised linear wheel deceleration η, the corresponding set-point value is $\overline{\eta}$. Also this control strategy has a straightforward graphical interpretation in the (λ, η) domain, as displayed in Figure 3.3, which shows again the equilibrium manifolds $\eta(\lambda)$ in four different road conditions.

From Figure 3.3 it is immediately clear which is the first major drawback of deceleration control: the selection of the set-point $\overline{\eta}$ is very critical, and it is impossible to find a unique value of $\overline{\eta}$ that provides a good compromise in every road condition. If a large value of $\overline{\eta}$ is chosen (*e.g.*, $\overline{\eta} = 1$), deceleration control provides optimal performance on high-grip road, but on low-grip roads the wheel dynamics do not exhibit any equilibrium point. On the other hand, a low value of $\overline{\eta}$ (*e.g.*, $\overline{\eta} = 0.1$) can guarantee the existence of an equilibrium for every road condition, but it results in an over-conservative design for high-grip roads. As has already been remarked (see Section 2.5.1), note that the system always has (if any) two equilibrium points.

To analyse the dynamic properties of the deceleration control system, we consider the transfer function model $G_\eta(s)$ given in Equation 2.45 in a unitary

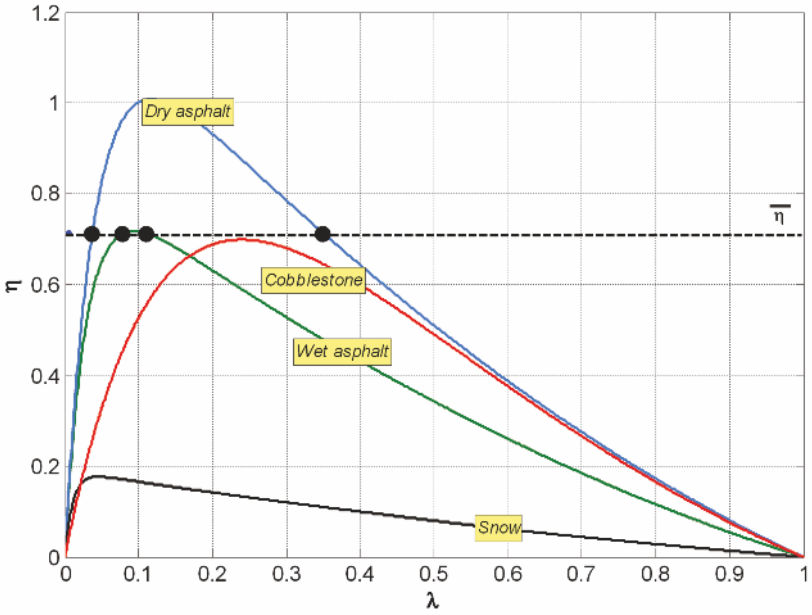

Figure 3.3 Graphical interpretation of deceleration control in the (λ, η) domain. The *horizontal dashed* line represents the set-point $\overline{\eta}$. The *dots* represent the equilibrium points, for different road conditions

negative feedback connection with a proportional controller with gain K, yielding the closed-loop system depicted in Figure 3.4.

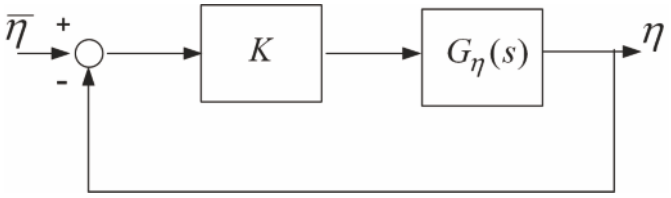

Figure 3.4 Wheel deceleration closed-loop system with a proportional controller

For this system, the characteristic polynomial $\chi_\eta(s)$ of the closed-loop system has the form

$$\chi_\eta(s) = \left(1 + K\frac{r}{Jg}\right)s + \frac{\mu_1(\overline{\lambda})F_z}{m\overline{v}}\left[(1-\overline{\lambda})\left(1 + K\frac{r}{Jg}\right) + \frac{mr^2}{J}\right].$$

Accordingly, the following stability condition can be derived (note that it does not depend on $\overline{v}$).

Stability Condition for Deceleration Control

The closed-loop stability condition for the deceleration control shown in Figure 3.4 is given by

$$\mu_1(\overline{\lambda}) \left[(1 - \overline{\lambda}) \left(1 + K \frac{r}{Jg} \right) + \frac{mr^2}{J} \right] > 0.$$

Clearly, it is not possible to find a fixed value of K that provides stability for every value of $\overline{\lambda}$ and for every road condition, since $\mu_1(\overline{\lambda})$ can be either positive or negative, depending on the value of $\overline{\lambda}$. Notice that if, *e.g.*, $K > 0$, the closed-loop system in Figure 3.2 can be made asymptotically stable for choices of $\overline{\lambda}$ before the friction curve peak, but it becomes unstable for choices of $\overline{\lambda}$ beyond the peak. Henceforth, one of the two equilibrium points is always unstable.

This analysis reveals the main limits of deceleration control:

- The choice of $\overline{\eta}$ is very critical; henceforth, it must be adapted online by means of an estimation algorithm which allows to detect the current road conditions.
- With a fixed structure controller (*i.e.*, with a fixed value of K), the asymptotic stability of the closed-loop linearised system is not guaranteed for all choices of $\overline{\lambda}$, also for a fixed road condition (this result can be extended from a simple proportional controller to every linear time-invariant controller).
- For wheel slip values beyond the peak of the friction curve the open-loop system is non-minimum phase (see Section 2.5.1 and the transfer function $G_\eta(s)$ in (2.45)) and this significantly limits the achievable closed-loop performance.

Due to these major drawbacks, deceleration control has never been implemented as a classical regulation loop for ABS in practice. Rather, complex rule-based heuristics based on a set of adjustable thresholds on η and its derivative have been used (see, *e.g.*, [88, 124]).

However, it is important to recall that deceleration-based algorithms have the appealing feature of requiring only the measurement of the wheel deceleration (no vehicle speed estimation is required). The wheel deceleration can be measured in a very reliable and straightforward manner with low cost sensors, the noise affecting the measure of η is almost stationary, and the variance of this noise can be *a priori* designed by properly choosing the precision of the wheel encoder (see also Appendix B).

Notice that deceleration control can be particularly appealing when the considered vehicle is such that its main dynamic limit during braking is not

due to the tyre–road friction but rather to the rollover condition, *e.g.*, the so-called *wheelie* phenomenon (that is the uplift of the rear wheel when braking on high-grip roads) in two-wheeled vehicles, which is mainly due to the large ratio between the height of the centre of mass and the wheelbase.

As has already been mentioned, the reader is referred to Chapter 6 for the illustration of a control strategy capable of properly *mixing* the benefits and drawbacks of slip and deceleration control and which leads to optmised performance of the resulting braking control system.

3.4 Linear Wheel Slip Controller Design

For the design of a linear wheel slip controller, we work on the transfer function model $G_\lambda(s)$, which is repeated here to ease readability

$$G_\lambda(s) = \frac{r}{J\overline{v}} \frac{1}{s + \frac{\mu_1(\bar{\lambda})F_z}{m\overline{v}} \left((1-\bar{\lambda}) + \frac{mr^2}{J}\right)}. \tag{3.2}$$

Further, as we are interested in the synthesis of a single controller capable of providing both closed-loop stability and acceptable performance in all working conditions, first of all we need to define the linearisation conditions based on which we can evaluate $G_\lambda(s)$ to serve as a basis for controller synthesis.

To do this, recall that the pole of the system can be written as

$$s_p = -\mu_1(\bar{\lambda}) \frac{Ng}{\overline{v}} \left((1-\bar{\lambda}) + \frac{mr^2}{J}\right), \tag{3.3}$$

thereby showing that the pole location depends on the vehicle speed v, on the vertical load distribution N, see also Equation 2.53, and on the road conditions.

Thus, to account for the load variations at the front and rear wheels (the former becomes more loaded during braking due to load transfer while the opposite is true for the latter) it is wise to tune the controllers for the front axle in a different way with respect to those that regulate the rear wheels.

Further, one needs to linearise the model around an open-loop unstable equilibrium point, so as to work on the *worst* case with respect to the road friction conditions. Thus, to investigate which is the most appropriate operating point in which to evaluate $G_\lambda(s)$, Figure 3.5 shows a plot of the system pole angular frequency as a function of λ for $N = 1.5$ (*i.e.*, in a setting compatible with the front wheel load) normalised with respect to the vehicle speed to capture the effects of load transfer and friction conditions only. To improve readability, and coherently with the aim of defining a worst-case setting, Figure 3.5 shows the pole angular frequency only for the open-loop

unstable equilibrium points (in the case where the real pole is negative, its angular frequency has been clipped to zero).

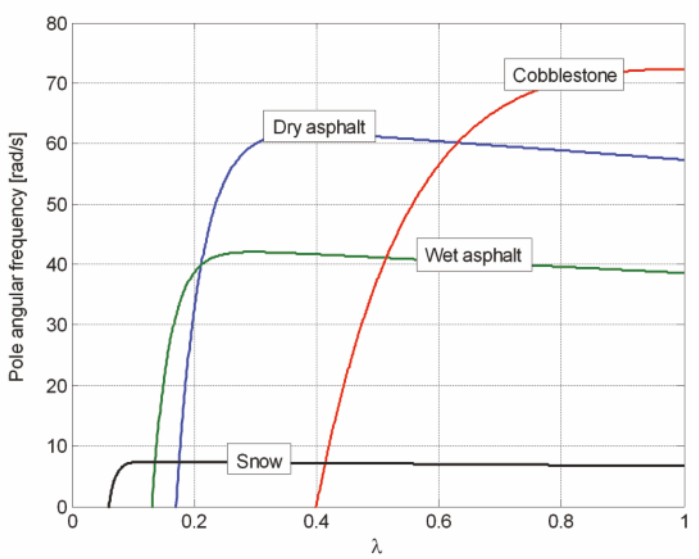

Figure 3.5 Angular frequency of the open-loop pole (3.3) normalised with respect to $\overline{v}$ for $N = 1.5$

By inspecting Figure 3.5 the following operating point for linearisation is considered. For the front wheel the worst-case situation considered for linearisation happens on dry asphalt, where the large value of N (see also Figure 2.11), causes the pole to move toward higher frequencies. Thus, on dry asphalt, for $\lambda = 0.62$ we obtain a pole $s_p = 60/\overline{v}$. Note that this is not the worst-case condition in general; by inspecting Figure 3.5 one may see that the pole location which is at the largest distance from the imaginary axis is found for $\lambda = 0.85$ on cobblestone. However, this situation, that is a very large value of the wheel slip on cobblestone, is much less likely to occur in practice. As such, choosing such a condition as a basis for controller design would be overly conservative. Of course, this choice is problem-dependent, and must be carefully evaluated according to the specific situation. On the other hand, whichever condition is chosen, the control designer will have to always check that basic closed-loop properties, such as asymptotic stability of the closed-loop system, are guaranteed in all admissible working conditions, possibly with a loss of dynamic performance with respect to the nominal case chosen for control design. A similar rationale may be applied to fix the linearisation point for the rear wheel if needed.

Based on these considerations, for controller design we will work with the transfer function $G_\lambda(s)$ given by

$$G_\lambda(s) = \frac{0.3/\overline{v}}{s - 60/\overline{v}} = \frac{\rho}{s + \gamma}, \tag{3.4}$$

with $\rho > 0$ and $\overline{v} > 0$.

Before moving to the design of a dynamic controller, let us recall that we have shown that with an appropriate choice of the controller gain value, a proportional controller which guarantees closed-loop stability for all working conditions can be found.

However, besides guaranteeing closed-loop stability, one usually needs to satisfy also performance specifications, which call for the design of a dynamic controller. The equilibria of the system to be controlled being open-loop unstable in some operating conditions of interest, there are two main approaches to the design of a performance-oriented controller. One choice may be that of designing first an internal feedback loop with the only aim of stabilising the closed-loop system in all operating conditions (note that this can be done, for example, with the simple proportional controller discussed previously) and then design an external control loop whose aim is to ensure the satisfaction of performance requirements and disturbance rejection properties. This approach allows one to work on a pre-stabilised system dynamics, which indeed poses less limitations on the achievable performance levels (for a detailed and advanced discussion on the limitations on closed-loop performance posed by right half plane poles and/or zeros the reader may refer to, *e.g.*, [98]).

The other option is that of designing a single controller which deals with both stabilisation and performance specifications. As in the considered application this second approach allows us to highlight some interesting tuning rules, in the following the design will be approached accordingly.

Thus, the first attempt to ensure, say, asymptotic tracking of a constant set-point (which is usually the first performance specification that one needs to fulfil) would lead to consider an integral controller, *i.e.*,

$$R_I(s) = \frac{K}{s}. \tag{3.5}$$

Consider, as an example, working on the transfer function model $G_\lambda(s)$ in (3.4) and employing the integral controller (3.5).

Assuming again unitary negative feedback, it is easy to see that the characteristic polynomial is given by

$$\chi_{\lambda(s),I} = s^2 + \gamma\, s + K\rho. \tag{3.6}$$

Thus, it is apparent that, in the case $\gamma < 0$, *i.e.*, if $G_\lambda(s)$ is open-loop unstable, no matter which value of K is chosen, the closed-loop system will never be asymptotically stable (recall that, the characteristic polynomial being a

second-order one, the necessary and sufficient condition for its roots to have negative real part is that all its coefficients are non-zero and have the same sign).

Bearing this in mind, let us move to consider a PI controller structure, *i.e.*,

$$R_{PI}(s) = K\frac{(\tau\, s + 1)}{s}, \tag{3.7}$$

with $\tau > 0$. With this controller, the characteristic polynomial (assuming again unitary negative feedback) is given by

$$\chi_{\lambda(s),PI} = s^2 + (K\rho\tau + \gamma)s + K\rho. \tag{3.8}$$

In this case, because $\rho > 0$ and $\tau > 0$, if K is chosen such that

$$K > -\frac{\gamma}{\rho\tau}, \tag{3.9}$$

then the closed-loop system will be asymptotically stable. Note that with a PI controller structure we obtained a closed-loop stability condition that is fully analogous to the one obtained for the proportional controller (see inequality (3.1)), with the additional degree of freedom offered by the time constant τ of the controller zero, which can be used, together with the controller gain K to guarantee that, besides closed-loop stability, other performance specifications are met. Substituting the full expressions for γ and ρ, see Equation 3.2, in (3.9), one obtains

$$K > -\mu_1(\bar{\lambda})\frac{NJg}{\tau r}\left((1-\bar{\lambda}) + \frac{mr^2}{J}\right), \tag{3.10}$$

which notably does not depend on the considered speed value $\overline{v}$ (recall that the same was true for condition (3.1) obtained based on the proportional controller). However, in practice a PI controller might not be enough to ensure that all desired performance specifications are met. Thus, as final analysis step, we consider a PID controller architecture complemented with a first-order filter to achieve a causal approximation of the ideal derivative term, *i.e.*,

$$R_{PID}(s) = K\frac{(\tau_1\, s + 1)(\tau_2\, s + 1)}{s(Ts + 1)}, \tag{3.11}$$

with $\tau_1 > 0$, $\tau_2 > 0$ and $T > 0$. This controller, with unitary negative feedback, yields the characteristic polynomial

$$\chi_{\lambda(s),PID} = T\, s^3 + (K\rho\tau_1\tau_2 + T\gamma + 1)s^2 + [\gamma + K\rho(\tau_1 + \tau_2)]s + K\rho. \tag{3.12}$$

Recalling that γ is the angular frequency of the system pole and letting $\gamma := 1/T_p$, if the real pole of the controller is chosen to be sufficiently fast, *i.e.*, if $T << |T_p|$, one has that $T\gamma \approx 0$. Let us consider this simplification, which

constitutes a tuning rule on its own, and recall that a necessary condition for the closed-loop stability of the considered third-order system is given by the coefficients of the characteristic polynomial (3.12) being all non-zero and with the same sign.

Based on these considerations, one obtains that the controller parameters must satisfy the following inequality:

$$K > -\frac{\gamma}{\rho(\tau_1+\tau_2)} = -\mu_1(\bar{\lambda})\frac{NJg}{r(\tau_1+\tau_2)}\left((1-\bar{\lambda})+\frac{mr^2}{J}\right). \tag{3.13}$$

Again, we have found a speed-independent stability condition, which can be satisfied acting on the larger number of controller parameters offered by the PID architecture.

Further, resorting to Routh's stability criterion (see, *e.g.*, [5]), one can investigate the additional conditions on the controller parameters that must be satisfied to fulfil the necessary and sufficient condition for closed-loop stability. Specifically, by constructing the Routh's table and recalling the assumption that $T\gamma \approx 0$, one finds that the only non-trivial additional condition on the controller parameters has the form

$$K > \frac{T-(\tau_1+\tau_2)}{\rho(\tau_1+\tau_2)\tau_1\tau_2}. \tag{3.14}$$

3.5 Effects of Actuator Dynamics

To move toward a more realistic situation consider, as an example, the transfer function model $G_\lambda(s)$ in (3.4) with, *e.g.*, $\overline{v} = 10$ m/s, and a proportional controller with gain $K = 1000$. It is easy to see that such a controller ensures closed-loop stability. However, $G_\lambda(s)$ is not a complete representation of the dynamics to be controlled. As a matter of fact, one has to consider the actuator dynamics. In this case, we assume that we are dealing with the EMB actuator servo-controlled dynamics $G_{\text{caliper}}(s)$ given in (1.4), which is a first-order linear time-invariant system with a pole at $\omega_{\text{act}} = 70$ rad/s and a pure delay $\tau = 10$ ms.

Bearing this in mind, the overall system dynamics to be controlled are given by

$$D(s) = G_{\text{caliper}}(s)G_\lambda(s). \tag{3.15}$$

It is now interesting to investigate how the proportional controller with gain $K = 1000$ that we assumed to have designed considering only the transfer function model $G_\lambda(s)$ in (3.4) with $\overline{v} = 10$ m/s behaves if we consider the full dynamics (3.15). It is clear that the choice of a proportional controller is a simplistic one, but the considerations remain unaltered for more complex

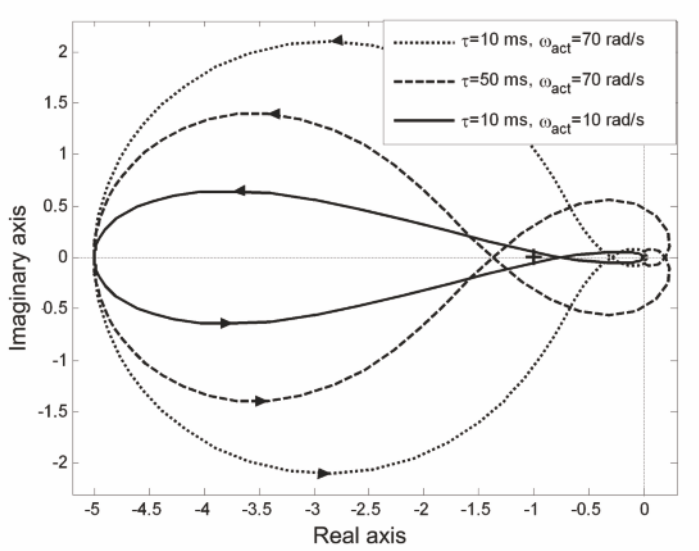

Figure 3.6 Nyquist diagram of the loop transfer function $L_\lambda(s)$ for $\tau = 10$ m/s and $\omega_{\rm act} = 70$ rad/s (*dotted line*), $\tau = 50$ m/s and $\omega_{\rm act} = 70$ rad/s (*dashed line*) and $\tau = 10$ m/s and $\omega_{\rm act} = 10$ rad/s (*solid line*)

controller structures. Such a simple choice is thus motivated by its ease of tractability.

For a pictorial representation of the considered situation, the reader is referred to Figure 3.6, which shows the Nyquist diagram of the loop transfer function

$$L_\lambda(s) = K\, D(s), \tag{3.16}$$

where $D(s)$ is as in (3.15) (and $K = 1000$), for different combinations of the actuator bandwidth and of the transmission delay.

Namely, the following situations are considered:

- the nominal case, *i.e.*, $\tau = 10$ ms and $\omega_{act} = 70$ rad/s (dotted line in Figure 3.6);
- a situation with a much larger transmission delay, *i.e.*, $\tau = 50$ ms and $\omega_{act} = 70$ rad/s (dashed line in Figure 3.6); and
- a situation with a much narrower actuator bandwidth, *i.e.*, $\tau = 10$ ms and $\omega_{act} = 10$ rad/s (solid line in Figure 3.6).

By inspecting Figure 3.6 it is clear that even though the controller gain chosen for the open-loop system $G_\lambda(s)$ still ensures stability for the nominal case of $\tau = 10$ ms and $\omega_{act} = 70$ rad/s, the same does not hold for the cases of a larger delay and of a narrower actuator bandwidth. Specifically, to cope with such modified situations one would in principle have to decrease the controller gain in order to ensure closed-loop stability, up to the point where

it would be impossible to fulfill condition (3.1) which ensures closed-loop stability for $G_\lambda(s)$ in all possible working conditions.

The message here is that one must always carefully evaluate all the system characteristics before moving to the controller design and investigate how and if they pose substantial limitations to the achievable closed-loop performance. If this is the case, then one may want to reconsider the vehicle layout or, if this is not possible, to revise the specifications and requirements for the closed-loop system.

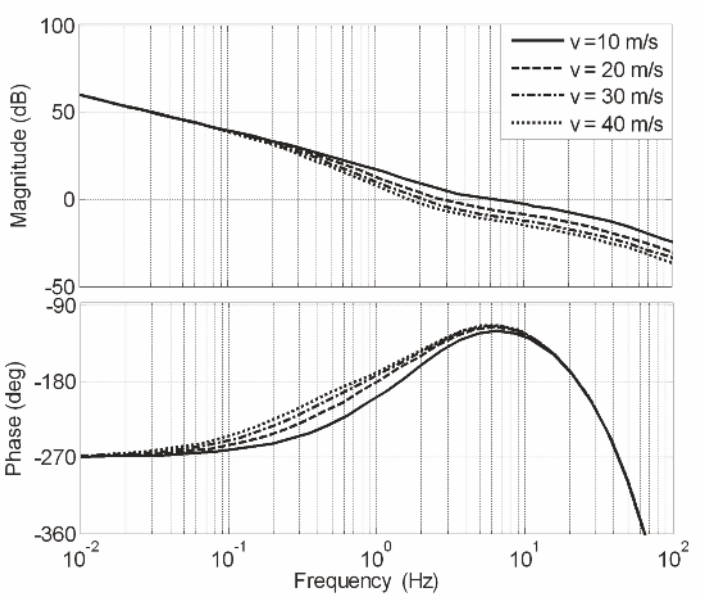

Figure 3.7 Magnitude and phase Bode diagrams of the frequency response associated with the loop transfer function $L_{1\lambda}(s)$ for $\overline{v} = 10$ m/s (*solid line*), $\overline{v} = 20$ m/s (*dashed line*), $\overline{v} = 30$ m/s (*dash-dotted line*) and $\overline{v} = 40$ m/s (*dotted line*)

3.6 Performance Analysis: a Numerical Example

We now design a slip controller that can achieve good dynamic performance, which, given the considered nominal actuator dynamics and transmission delay (*i.e.*, $\omega_{act} = 70$ rad/s and $\tau = 10$ ms), can be defined as: ensure asymptotic tracking of a constant wheel slip set-point and achieve a closed-loop bandwidth between approximately 1 and 10 Hz for all admissible speed values.

Based on the previous analysis, a PID controller architecture that satisfies the desired requirements can be devised. Note that besides fulfilling the stability conditions discussed in the previous section one has to consider the phase loss due to the delay and to the actuator dynamics.

In particular, the following PID controller can be employed:

$$R_\lambda(s) = 12000 \frac{(1 + \frac{1}{20}s)^2}{s(1 + \frac{1}{500}s)}. \tag{3.17}$$

Note that the controller (3.17) is not intended as the best possible tuning for the considered situation, but is given as an example of a simple controller architecture that achieves the desired performance levels. Each specific practical situation will lead to a more detailed list of requirements, which in turn will require a different tuning of the controller parameters.

To visually inspect the loop transfer function obtained with the controller (3.17), *i.e.*,

$$L_{1\lambda}(s) = R_\lambda(s)\, D(s), \tag{3.18}$$

the reader is referred to Figure 3.7, which shows the magnitude and phase Bode diagrams of the frequency response associated with $L_{1\lambda}(s)$ for different values of the vehicle speed. As can be seen the closed-loop bandwidth does indeed vary according to the vehicle speed value $\overline{v}$ used to evaluate the system dynamics $G_\lambda(s)$ in (3.4); specifically, the closed-loop dynamics are faster as speed decreases. Of course, no stability property of the closed-loop linearised system can be inferred from the Bode diagrams, as the loop transfer function has a positive pole.

The fact that the system dynamics become faster as speed decreases, coupled with the presence of a pure delay, makes it impossible to ensure closed-loop stability for very low values of $\overline{v}$.

To visually inspect this issue consider Figure 3.8, which shows the magnitude and phase Bode diagrams of the frequency response associated with the loop transfer function

$$L_{2\lambda}(s) = R_\lambda(s) D^{\mathrm{st}}(s),$$

where

$$D^{st}(s) = G_{\mathrm{caliper}}(s) G^{\mathrm{st}}_\lambda(s)$$

is the system dynamics obtained considering an open-loop stable equilibrium, that is

$$G^{\mathrm{st}}_\lambda(s) = \frac{0.3/\overline{v}}{s + 60/\overline{v}},$$

for $\overline{v} = 40$ m/s and $\overline{v} = 2$ m/s. As the loop transfer function has no poles with positive real part and the cut-off frequency is well-defined, the closed-loop stability can now be inferred *via* the Bode criterion. By inspecting Figure 3.8 one notes that for $\overline{v} = 2$ m/s the closed-loop system is unstable. Note that this is not due to the particular controller tuning; any controller tuning will

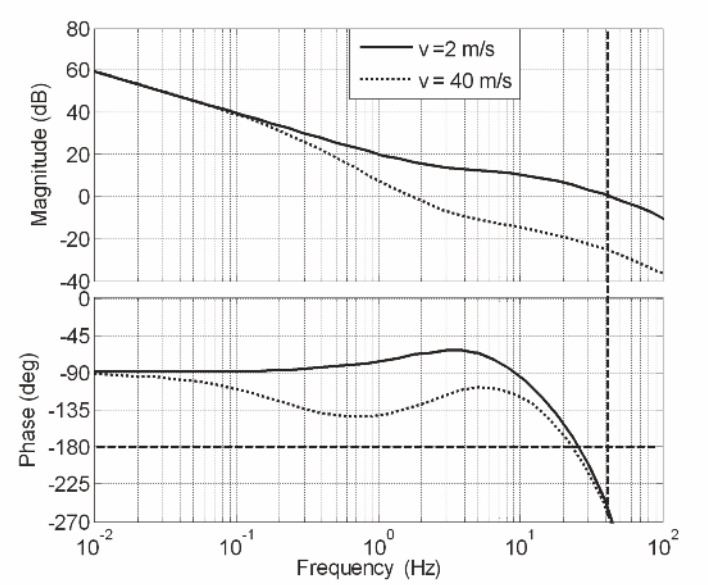

Figure 3.8 Magnitude and phase Bode diagrams of the frequency response associated with the loop transfer function $L_{2\lambda}(s)$ for $\overline{v} = 40$ m/s (*dotted line*) and $\overline{v} = 2$ m/s (*solid line*)

lead to a different minimum value of the speed which compromises closed-loop stability, but such a value will always exist.

Moreover, from a practical viewpoint one must also consider that at very low speed the wheel encoders used to measure the wheel speed become less reliable, so that the available wheel speed measurement cannot be safely employed to estimate the vehicle speed needed to compute the wheel slip. For a better analysis of these issues the reader is referred to Appendix B and to Chapter 5, which discuss the processing issues of the wheel encoders signal and the speed estimation problem, respectively.

In view of these problems, in practical applications the braking control system needs to be complemented with a deactivation logic that switches to an open-loop control strategy to manage the last part of the braking phase associated with very low values of the vehicle speed. The design of such a logic is addressed in the next section.

3.7 Activation and Deactivation Logic

The last design step, crucial for moving toward a real vehicle implementation, is to devise a safe and reliable activation and deactivation logic. As a matter

of fact, an active braking controller is a safety system, hence it is not active during normal vehicle operations but it has to be turned on when a panic stop occurs.

The first step is then to single out which signals better describe the current safety level on board as far as braking is concerned. Further, we need to devise an activation and deactivation logic based on these signals and take care that a bumpless transfer is guaranteed between manual and automatic operational modes.

To this end, the first step is to implement the wheel slip controllers with anti-windup architecture and with the structure shown in Figure 3.9, which ensures that a reliable controller output is available also when in manual mode, and that a bumpless transfer from manual to automatic mode is ensured upon the controller activation. The anti-windup implementation of the integral controller action is also necessary to cope with actuator constraints, which are of course to be taken into account in the considered application (see also Section 1.3).

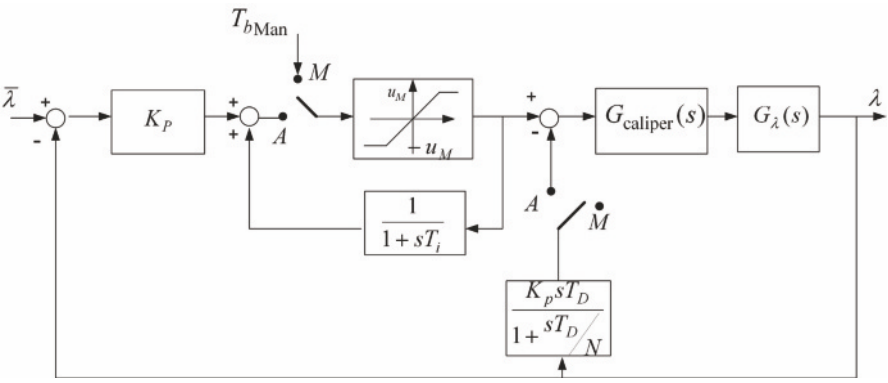

Figure 3.9 Schematic view of the implementation of a wheel slip PID controller which ensures a bumpless transfer from manual to automatic mode

Moreover, in the considered system, besides switching from manual to automatic mode, one has to monitor the value of the vehicle speed. In fact, in view of the analysis performed, when the value of the vehicle speed goes below a certain threshold, specific braking strategies must be devised in order to take the vehicle to a complete stop. Based on these considerations, the activation and deactivation logic is governed by the finite state machine (FSM) shown in Figure 3.10. We now analyse the conditions based on which the transitions between the states are activated.

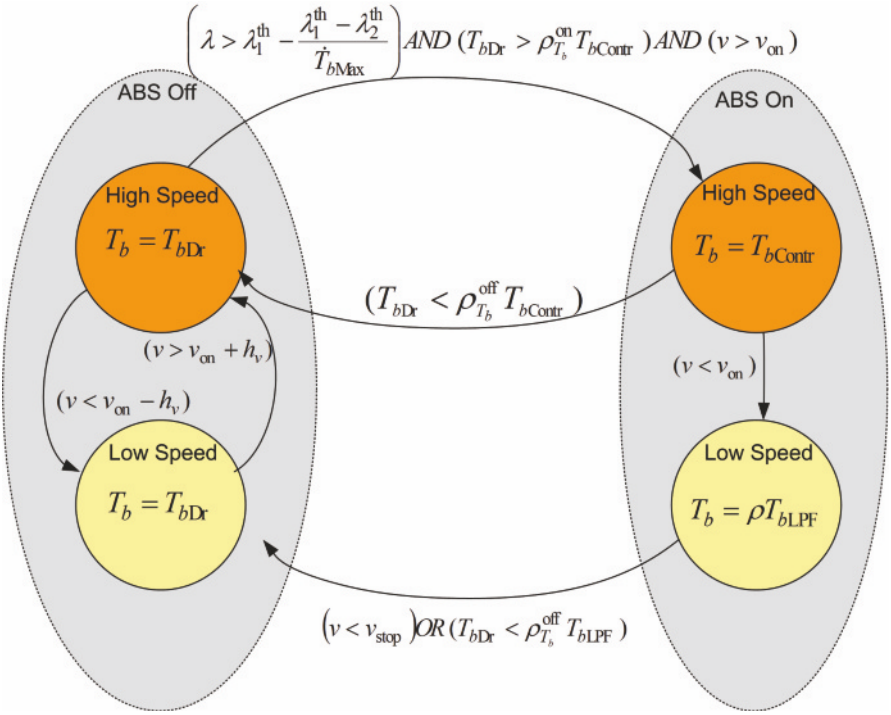

Figure 3.10 FSM representation of the activation and deactivation logic

3.7.1 Activation Conditions

When a braking manoeuvre takes place, the ABS is activated if the following condition holds (see also Figure 3.10 and Table 3.1):

$$\left(\lambda > \lambda_1^{\text{th}} - \frac{\lambda_1^{\text{th}} - \lambda_2^{\text{th}}}{\dot{T}_{b\text{Max}}} \dot{T}_b\right) \text{ AND } \left(T_{b\text{Dr}} > \rho_{T_b}^{\text{on}} T_{b\text{Contr}}\right) \text{ AND } (v > v_{\text{on}}) . \tag{3.19}$$

Thus, the activation is based on the wheel slip λ, the braking torque T_b and the vehicle speed v.

Specifically, the threshold on λ is modulated according to the braking intensity, described *via* the braking torque derivative $\dot{T}_b$. The threshold λ_1^{th} is employed in the case $\dot{T}_b = 0$, while a lower threshold value λ_2^{th} is used in the case when a hard braking manoeuvre occurs, *i.e.,* $\dot{T}_b = \dot{T}_{\text{bMax}}$. The first condition of (3.19) is simply a linear interpolation of these extreme conditions, which allows us to handle all the intermediate braking intensities.

However, note that an activation based only on this condition is not completely safe. In fact, the wheel slip λ is a noisy signal, and one needs to avoid that the controller is switched on due to possibly large measurement errors.

This is achieved by considering also the value of the braking torque, as shown by the second condition of (3.19), where $T_{b\mathrm{Dr}}$ is the braking torque requested by the driver, $T_{b\mathrm{Contr}}$ is the braking torque that the controller would apply if active (recall the the chosen controller architecture makes the control output available also in manual mode) and the parameter $\rho_{T_b}^{\mathrm{on}} > 1$.

Finally, as the controller is not guaranteed to ensure closed-loop stability at very low speed values, the automatic mode has to be switched on only if the speed value is sufficiently large, *i.e.*, if $v > v_{\mathrm{on}}$, where v_{on} is a properly defined threshold.

3.7.2 De-activation Conditions

When the braking manoeuvre is completed, the controller must be switched off so that the full control of the vehicle returns to the driver. Hence, an automatic to manual switch must occur when the driver releases the brake pedal. Thus, if the de-activation occurs at $v > v_{\mathrm{on}}$, it is allowed when the following condition holds (see again Figure 3.10):

$$T_{b\mathrm{Dr}} < \rho_{T_b}^{\mathrm{off}} T_{b\mathrm{Contr}}, \qquad \rho_{T_b}^{\mathrm{off}} < 1.$$

To switch off the controller at low speed, note that if the condition $v \leq v_{\mathrm{on}}$ occurs when a panic stop is still going on, then it is not safe to give back the control to the driver immediately. Hence, an additional braking logic has to be devised in order to take the vehicle to a complete stop automatically.

One solution is to complete the braking manoeuvre commanding the actuator to apply a constant braking torque, such that

$$T_b = \rho\, T_{b\mathrm{LPF}}, \qquad \rho < 1,$$

where $T_{b\mathrm{LPF}}$ is a low pass filtered version of the last value of the braking torque requested by the controller.

Then, once the vehicle has stopped or if the driver has released the brake pedal, *i.e.*, if

$$(v < v_{\mathrm{stop}})\,\mathrm{OR}\,(T_{b\mathrm{Dr}} < \rho_{T_b}^{\mathrm{off}}\, T_{b\mathrm{LPF}}),$$

then the ABS can be switched off (see the transition between the ABS on and off states associated with the low speed condition in Figure 3.10).

Figures 3.11(a) and 3.11(b) and Figures 3.12(a) and 3.12(b) show the closed-loop behaviour of the wheel slip and braking torque when the controller endowed with the activation logic is employed.

Specifically, Figures 3.11(a) and 3.11(b) show the results on dry asphalt, whereas Figures 3.12(a) and 3.12(b) those on snow. These figures show that the controller allows one to perform a safe braking manoeuvre and that the activation and deactivation logic guarantees a bumpless transfer between

Table 3.1 Description of the parameters employed in the activation and deactivation logic

Parameter	Value	Constraints	Meaning
$\rho_{T_b}^{\text{off}}$	0.9	< 1	Safety scaling between $T_{b\text{Dr}}$ and $T_{b\text{Contr}}$ to determine if the controller can be switched off at low speed
$\rho_{T_b}^{\text{on}}$	1.02	> 1	Scaling between $T_{b\text{Dr}}$ and $T_{b\text{Contr}}$ to activate the controller
ρ	0.97	< 1	Controller torque scaling factor for $v < v_{\text{on}}$
λ_1^{th}	0.2	$> \lambda_2^{\text{th}}$	Activation threshold for constant T_b
λ_2^{th}	0.1	> 0	Activation threshold for $\dot{T}_b = \dot{T}_{b\text{Max}}$
$\dot{T}_{b\text{Max}}$	5 kNm/s	> 0	Actuator rate limit
v_{on}	2.5 m/s	> 0	Speed threshold above which $T_{b\text{Contr}}$ is reliable
v_{stop}	0.05 m/s	$0 < v_{\text{stop}} \leq v_{\text{on}}$	Speed threshold below which the vehicle is considered still
h_v	0.5 m/s	> 0	Hysteresis on v_{on} to avoid chattering between the two manual ABS-OFF states

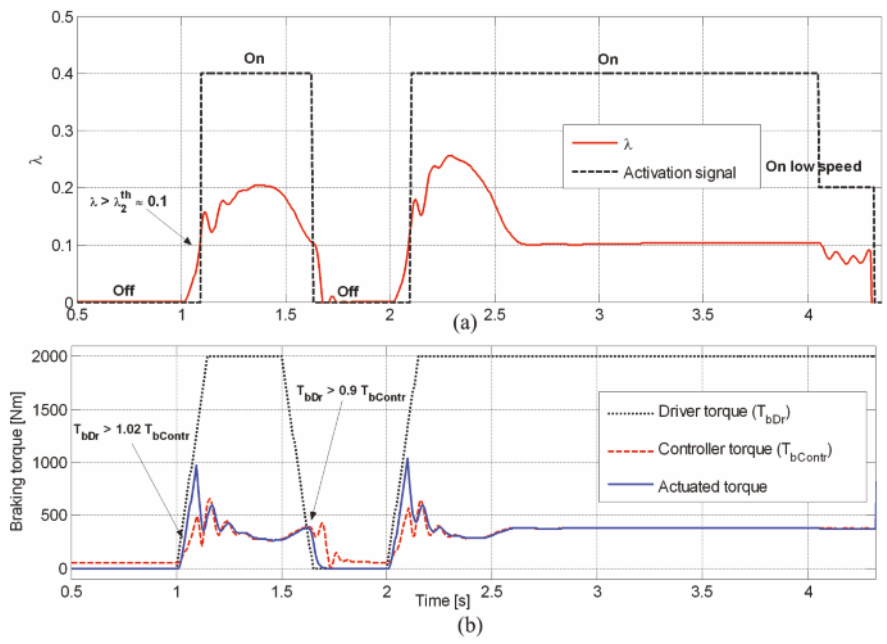

Figure 3.11 Activation logic behaviour for repeated braking manoeuvres on dry asphalt road with initial speed $v_0 = 100$ km/h; (a): plot of the longitudinal wheel slip (*solid line*) and activation signal (*dashed line*); (b): braking torque

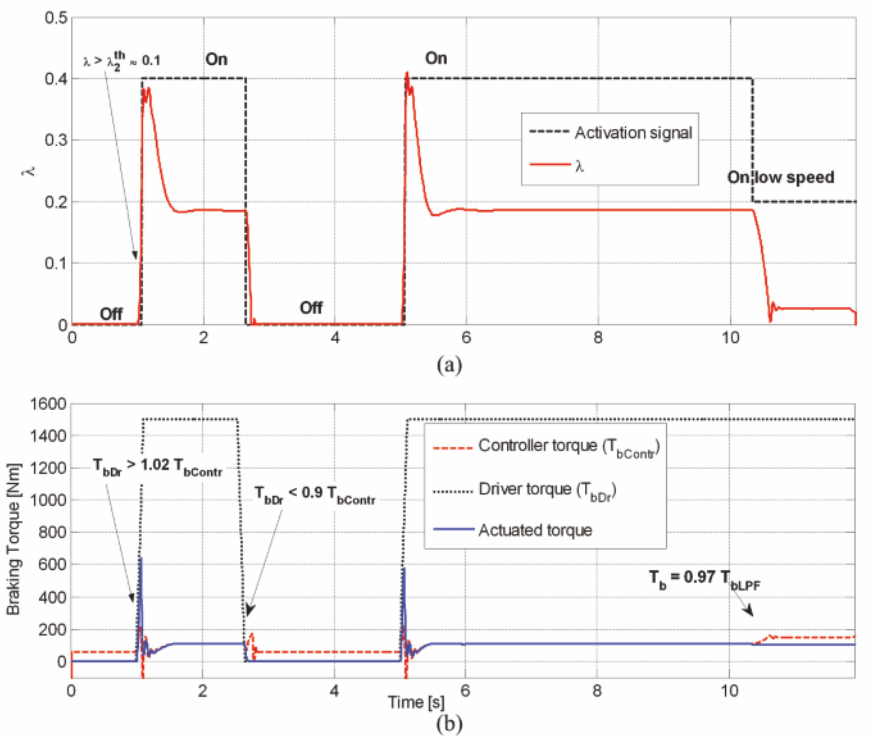

Figure 3.12 Activation logic behaviour for repeated braking manoeuvres on snowy road with initial speed $v_0 = 100$ km/h; (a): plot of the longitudinal wheel slip (*solid line*) and activation signal (*dashed line*); (b): braking torque

manual and automatic mode, and the controller state is correctly reset on deactivation, so that the subsequent braking manoeuvre can be safely handled. Finally, good performance and safety are ensured independently of the road condition.

In the simulations considered, the activation logic was implemented with the numerical values given in Table 3.1.

3.8 Slip Controller Analysis Based on the Double-corner Model

This section is devoted to investigating the wheel slip control problem starting from a double-corner model. Specifically, we first analyse the closed-loop stability properties obtained with a slip controller acting on both the front and the rear wheels. Further, we discuss an alternative control strategy that interlocks the rear wheels with the front ones, and allows one on the one

hand to achieve coupling minimisation while maintaining a SISO approach to wheel slip control and on the other hand to employ a control strategy that does not need the rear wheel slip measurement.

Finally, we briefly discuss the problem of adapting a wheel slip control system to the case of braking on curves, showing that the approaches discussed in this book still apply if the current manoeuvre does not compromise the vehicle stability, provided that a set-point adaptation strategy is available.

3.8.1 Closed-loop Stability Analysis

Similarly to what was done at the beginning of this chapter on the single-corner model, we now analyse the closed-loop stability of the wheel slip control applied to the double-corner model given in system (2.25).

Specifically, to perform the analysis it is assumed that the longitudinal dynamics of the vehicle (expressed by the state variable v) are significantly slower than the rotational dynamics of the wheels (expressed by the state variables λ_i or ω_i, $i = \{f, r\}$) due to the differences in inertia. Under this assumption, the third equation (centre of mass dynamics) in (2.25) is neglected, and the model reduces to a second-order model of the wheels dynamics only where v is treated as a varying parameter.

Further, as it was done for the single-corner model, we concentrate for simplicity on a proportional controller. This choice allows us to draw general conclusions, which hold also with a more complex linear time-invariant controller.

Finally, based on the analysis carried out in Chapter 2 (see also Figures 2.12(a) and 2.12(b)), which revealed that the front wheel behaviour is substantially independent from that of the rear wheel, while the latter is strongly coupled to the front one, in the following we disregard the dependence of $\Psi_f(\lambda_f, \lambda_r)$, see Equation 2.26, on λ_r and adopt the notation $\Psi_f(\lambda_f)$.

Accordingly, the control laws obtained with a proportional controller applied to each wheel have the form

$$\begin{aligned} T_{b_f} &= k_f(\overline{\lambda}_f - \lambda_f), \\ T_{b_r} &= k_r(\overline{\lambda}_r - \lambda_r), \end{aligned} \tag{3.20}$$

where $\overline{\lambda}_f$ and $\overline{\lambda}_r$ are the set-point values for the front and rear wheel slip, respectively, and k_f, k_r are positive constants. Hence, the closed-loop dynamics become

$$\begin{aligned} \dot{\lambda_f} &= -\frac{r}{Jv}\left[\Psi_f(\lambda_f) - k_f(\overline{\lambda}_f - \lambda_f)\right], \\ \dot{\lambda_r} &= -\frac{r}{Jv}\left[\Psi_r(\lambda_f, \lambda_r) - k_r(\overline{\lambda}_r - \lambda_r)\right]. \end{aligned} \tag{3.21}$$

For the closed-loop system (3.21), we can state the following:

Proposition 3.1. *Consider the closed-loop system described by* (3.21) *with* $v > 0$ *and let the wheel slip set-point values be* $\overline{\lambda}_i \in (0,1)$, $i = \{r, f\}$. *Then, there exist positive gain values* $\overline{k}_f$ *and* $\overline{k}_r$ *such that, for any* $k_f > \overline{k}_f$ *and* $k_r > \overline{k}_r$, *the closed-loop system admits a unique locally asymptotically stable equilibrium for all initial conditions* $\lambda_f(0), \lambda_r(0) \in (0,1)$, *for all choices of* $\overline{\lambda}_f$ *and* $\overline{\lambda}_r$ *and for all road conditions.*

Proof. Fix the set-point values $\overline{\lambda}_f, \overline{\lambda}_r \in (0,1)$. As a proportional controller does not guarantee that the wheel slip of the closed-loop system will converge to $\overline{\lambda}_f, \overline{\lambda}_r$, let $(\tilde{\lambda}_f, \tilde{\lambda}_r)$ be an equilibrium of system (3.21) associated with $\overline{\lambda}_f, \overline{\lambda}_r$, *i.e.*,

$$\begin{cases} \Psi_f(\tilde{\lambda}_f) = k_f(\overline{\lambda}_f - \tilde{\lambda}_f), \\ \Psi_r(\tilde{\lambda}_f, \tilde{\lambda}_r) = k_r(\overline{\lambda}_r - \tilde{\lambda}_r). \end{cases} \tag{3.22}$$

As a preliminary step, we re-write system (3.21) in a form that is more useful for analysing the stability properties of $(\tilde{\lambda}_f, \tilde{\lambda}_r)$.

We start from the equation governing λ_r, which can be expressed in the form

$$\begin{aligned} \dot{\lambda_r} &= -\frac{r}{Jv}\Big\{k_r(\lambda_r - \tilde{\lambda}_r) + \Psi_r(\tilde{\lambda}_f, \lambda_r) - k_r(\overline{\lambda}_r - \tilde{\lambda}_r) \\ &\quad + \Psi_r(\lambda_f, \lambda_r) - \Psi_r(\tilde{\lambda}_f, \lambda_r)\Big\} \\ &= -\frac{r}{Jv}\Big\{(\lambda_r - \tilde{\lambda}_r)\Big[k_r + \frac{\Psi_r(\tilde{\lambda}_f, \lambda_r) - \Psi_r(\tilde{\lambda}_f, \tilde{\lambda}_r)}{\lambda_r - \tilde{\lambda}_r}\Big] \\ &\quad + \Psi_r(\lambda_f, \lambda_r) - \Psi_r(\tilde{\lambda}_f, \lambda_r)\Big\}, \end{aligned}$$

where the first equality is obtained by adding and subtracting $k_r\tilde{\lambda}_r$ and $\Psi_r(\tilde{\lambda}_f, \lambda_r)$ to the expression within the brackets in (3.21), whereas the second equality is obtained using the equilibrium condition (3.22).

A similar procedure applied to the equation governing λ_f in (3.21) leads to the following equivalent form for the closed-loop system equations:

$$\begin{aligned} \dot{\lambda_f} &= -\frac{r}{Jv}\Big[k_f + \alpha_f(\lambda_f)\Big](\lambda_f - \tilde{\lambda}_f), \\ \dot{\lambda_r} &= -\frac{r}{Jv}\Big[k_r + \alpha_r(\lambda_r)\Big](\lambda_r - \tilde{\lambda}_r) + \gamma(\lambda_f, \lambda_r), \end{aligned} \tag{3.23}$$

where

$$\alpha_f(\lambda_f) = \frac{\Psi_f(\lambda_f) - \Psi_f(\tilde{\lambda}_f)}{\lambda_f - \tilde{\lambda}_f},$$

$$\alpha_r(\lambda_r) = \frac{\Psi_r(\tilde{\lambda}_f, \lambda_r) - \Psi_r(\tilde{\lambda}_f, \tilde{\lambda}_r)}{\lambda_r - \tilde{\lambda}_r},$$

and

$$\gamma(\lambda_f, \lambda_r) = -\frac{r}{Jv}[\Psi_r(\lambda_f, \lambda_r) - \Psi_r(\tilde{\lambda}_f, \lambda_r)].$$

Note that the system under study is made of a cascade connection of two subsystems where λ_f evolves independently of λ_r and this affects the dynamics of λ_r through the additive term $\gamma(\lambda_f, \lambda_r)$, which vanishes when λ_f is at the equilibrium, *i.e.*, $\gamma(\tilde{\lambda}_f, \lambda_r) = 0$, $\forall \lambda_r$. Also, $\alpha_f(\lambda_f)$ represents the slope of the straight line intersecting the curve $\Psi_f(\cdot)$ in the two points of coordinates λ_f and $\tilde{\lambda}_f$. Thus, $\alpha_f(\lambda_f)$ is lower bounded by the negative steepest slope of the curve $\Psi_f(\cdot)$ obtained for different road conditions. A similar geometric interpretation holds for $\alpha_r(\lambda_r)$.

It is next shown that, for $i \in \{f, r\}$, if k_i is large enough, then the equilibrium $\tilde{\lambda}_i$ of the subsystem

$$\dot{\lambda_i} = -\frac{r}{Jv}\Big[k_i + \alpha_i(\lambda_i)\Big](\lambda_i - \tilde{\lambda}_i) \tag{3.24}$$

is globally exponentially stable (GES) and, hence, also globally asymptotically stable (GAS). Note that subsystem (3.24) with $i = r$ is obtained from the cascade system (3.23) by removing the interconnection term $\gamma(\lambda_f, \lambda_r)$ and setting λ_f at the equilibrium.

Consider the candidate Lyapunov function

$$V(\lambda_i) = \frac{(\lambda_i - \tilde{\lambda}_i)^2}{2},$$

which, by construction, is positive definite ($V(\lambda_i) > 0$ for all $\lambda_i \neq \tilde{\lambda}_i$, and $V(\tilde{\lambda}_i) = 0$) and is radially unbounded. The time derivative of V along the subsystem trajectories is

$$\dot{V}(\lambda_i) = (\lambda_i - \tilde{\lambda}_i)\dot{\lambda}_i = -\frac{r}{Jv}\Big[k_i + \alpha_i(\lambda_i)\Big](\lambda_i - \tilde{\lambda}_i)^2.$$

Thus, recalling the definition of $\alpha_f(\lambda_f)$ and $\alpha_r(\lambda_r)$, if

$$k_f > \bar{k}_f = -\min_{\vartheta, \lambda_f, \lambda'_f} \frac{\Psi_f(\lambda_f) - \Psi_f(\lambda'_f)}{\lambda_f - \lambda'_f}, \tag{3.25}$$

$$k_r > \bar{k}_r = -\min_{\vartheta, \lambda_r, \lambda'_r, \lambda'_f} \frac{\Psi_r(\lambda'_f, \lambda_r) - \Psi_r(\lambda'_f, \lambda'_r)}{\lambda_r - \lambda'_r}, \tag{3.26}$$

one obtains that $\dot{V}(\lambda_i) < -c_i(\lambda_i - \tilde{\lambda}_i)^2$, with $c_i > 0$, which concludes the proof that the equilibrium $\tilde{\lambda}_i$ of subsystem (3.24) is GES (see also Appendix A). The stability properties of the equilibria of two nonlinear subsystems ensure that, once the cascade interconnection of the two is active, the closed-loop system admits a unique equilibrium point that is locally asymptotically stable (see *e.g.*, [44]).

□

Note that, in the case of nonlinear systems, the global asymptotic stability of the equilibrium of each of the two subsystems is not enough to infer the same property for the equilibrium of the interconnection, while this is instead true for the cascade connections of linear systems, see, *e.g.*, [35].

Note further that a solution to the equilibrium conditions (3.22) always exists for all gain values $k_f, k_r > 0$ and it can be graphically identified by first intersecting $\Psi_f(\lambda_f)$ in Figure 2.12(a) with the line of negative slope $-k_f$ cutting the λ_f axis in $\overline{\lambda}_f$ to determine $\tilde{\lambda}_f$, and then intersecting $\Psi_r(\tilde{\lambda}_f, \lambda_r)$ in Figure 2.12(b) with the line of negative slope $-k_r$ cutting the λ_r axis in $\overline{\lambda}_r$ to determine $\tilde{\lambda}_r$. If k_f and k_r satisfy the bound for the global asymptotic stability to hold, the equilibrium is unique. Note also that, as we are using a proportional controller, the values $\tilde{\lambda}_f$ and $\tilde{\lambda}_r$ are in general different from the set-point values $\overline{\lambda}_f$ and $\overline{\lambda}_r$. From the equilibrium conditions (3.22), however, it is clear that $\tilde{\lambda}_f$ and $\tilde{\lambda}_r$ can be made close to $\overline{\lambda}_f$ and $\overline{\lambda}_r$ if the controller gains k_r and k_f are sufficiently large.

Finally, it is worth pointing out that the condition obtained on the controller gains is similar to that given for the single-corner model in Section 3.2, where it was shown that the gain must be larger than the steepest negative slope of the friction curve for all road conditions to ensure *local* stability. Proposition 3.1 thus extends the results obtained on the single-corner model to the double-corner one, and from a linear to a nonlinear analysis setting.

3.8.2 Controlling the Rear Wheel: Slip versus Relative Slip Control

The double-corner model analysis has shown that stability can indeed be guaranteed with results that are fully analogous to those obtained with the single-corner model. The dynamic analysis carried out in Section 2.5.2 warned us that a dynamic coupling is present between front and rear wheel, which can be more or less significant according to the specific vehicle characteristics. In general, it cannot be neglected in vehicles that experience a very large load transfer between front and rear axles during braking, such as two-wheeled vehicles.

As an example, consider Figure 3.13, which shows the typical behaviour of the longitudinal force F_x as a function of the wheel slip at the front and rear wheels in a vehicle with large load transfer. As discussed in Section 2.2, the longitudinal force scales with the vertical load F_z and also the peak value shifts forward in λ as F_z increases due to the non-exact proportionality between F_z and F_x. So, assuming that one wants to control the wheel slip of both wheels at the value $\overline{\lambda}$ shown in Figure 3.13, the control problem at the rear wheel is difficult to be handled in open-loop by the driver, as $\overline{\lambda}$ is

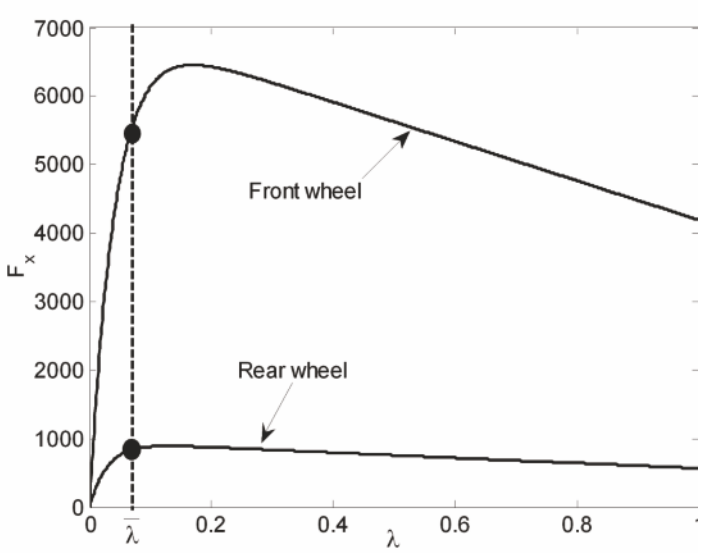

Figure 3.13 Longitudinal force as a function of the wheel slip at the front and rear wheels in a vehicle with large load transfer

very close to the peak of the friction curve, while this is not true for the front wheel.

As such, especially with two-wheeled vehicles, in the situation depicted in Figure 3.13 one would have the front wheel slip left in open-loop to be regulated by the driver, whereas the rear wheel slip should be regulated in closed-loop by an active controller.

Based on the above considerations, the idea is to devise an alternative control strategy for the rear wheel. The solution that we propose is that of considering an alternative control variable for the rear wheel, based on the idea of interlocking the rear wheels with the front ones with the aim of guaranteeing the same wheel slip on both axles.

Specifically, the controlled variable for the rear wheel is the speed difference between front and rear wheel, *i.e.*,

$$\omega_f - \omega_r, \tag{3.27}$$

which can be linked to slip control by means of the following equality:

$$\omega_f - \omega_r = \frac{v}{r}(\lambda_f - \lambda_r). \tag{3.28}$$

Hence, if we achieve $\omega_f - \omega_r = 0$, this implies that also the wheel slip at front and rear wheels will be the same. This is why we will refer to this approach as *relative slip control*.

Formulating the rear wheel control problem as that of regulating to zero the relative slip offers significant advantages with respect to controlling the rear wheel slip. First of all, feedback based on (3.27) does not require a measurement of the wheel slip. This is a particularly important feature in two-wheeled vehicles, where slip estimation is more critical than in cars, due to the larger load transfer. Thus, in the case where the front wheel slip is regulated by the driver, relative slip control at the rear wheel can be implemented by simply having two wheel encoders, which provide a cheap and robust measurement.

Further, from a dynamic viewpoint, Equation 3.28 reveals that the dependence on the forward speed obtained using the relative slip is different from the one obtained using the wheel slip as controlled variable.

Specifically, to compute the transfer function $G_{\omega_r-\omega_r}(s)$ from the rear braking torque δT_{br} to $\delta(\omega_f - \omega_r)$ of the double-corner model, the second-order state space representation employed in Section 2.5.2 can be used again with only the modification of the C matrix, which in view of (3.28) takes the form

$$C = \begin{bmatrix} 1 & 0 \\ -\frac{\overline{v}}{r} & \frac{\overline{v}}{r} \end{bmatrix}.$$

Thus, if we assume again, as was done in Section 2.5.2, that we can disregard the dependence of $\Psi_f(\lambda_f, \lambda_r)$ from λ_r and set $\delta\overline{\Psi}_{f,r} = 0$, the transfer function $G_{\omega_r-\omega_r}(s)$ is given by

$$G_{\omega_r-\omega_r}(s) = \frac{1}{J}\frac{s + \frac{r}{J\overline{v}}\delta\overline{\Psi}_{f,f}}{D(s)}, \tag{3.29}$$

where $D(s)$ is as in (2.71). Hence, the dependence of $G_{\omega_r-\omega_r}(s)$ on $\overline{v}$ is significantly different from that of $G_{rr}(s)$. Specifically, the static gain is given by

$$G_{\omega_r-\omega_r}(0) \cong \frac{\overline{v}J/r}{\delta\overline{\Psi}_{r,r}}, \tag{3.30}$$

thus proportional to the vehicle speed, while that of $G_{rr}(s)$ was independent of $\overline{v}$, see Equation 2.74. The high frequency gain, instead, is given by

$$\lim_{s\to\infty} s\, G_{\omega_r-\omega_r}(s) = \frac{1}{J}, \tag{3.31}$$

thus independent of $\overline{v}$, while that of $G_{rr}(s)$ was inversely proportional to $\overline{v}$, see Equation 2.78.

Figures 3.14(a) and 3.14(b) show a comparison between the Bode plots of the frequency responses associated with $G_{rr}(s)$ and with $G_{\omega_r-\omega_r}(s)$ obtained employing the double-corner model (see Section 2.4) with $\overline{\lambda_r} = 0.05$, $\overline{v} = 25$ m/s and on dry asphalt for different vehicle speed values, which visually confirm the different dynamic behaviour just analysed. Based on these results,

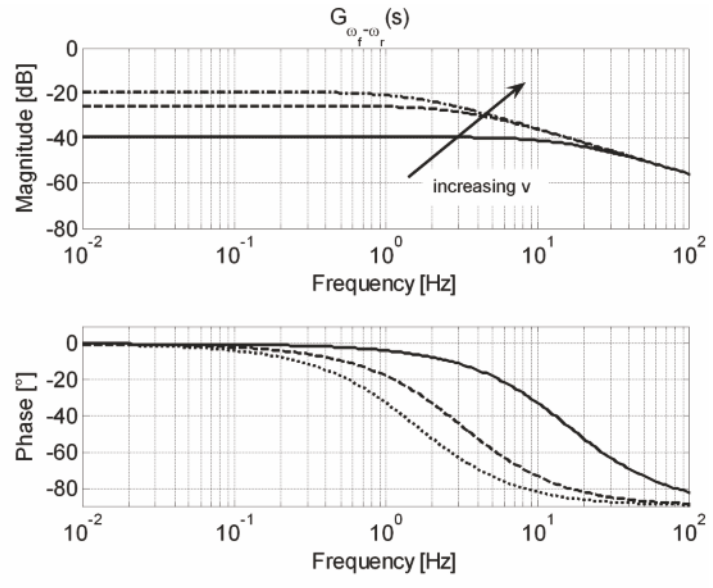

(a)

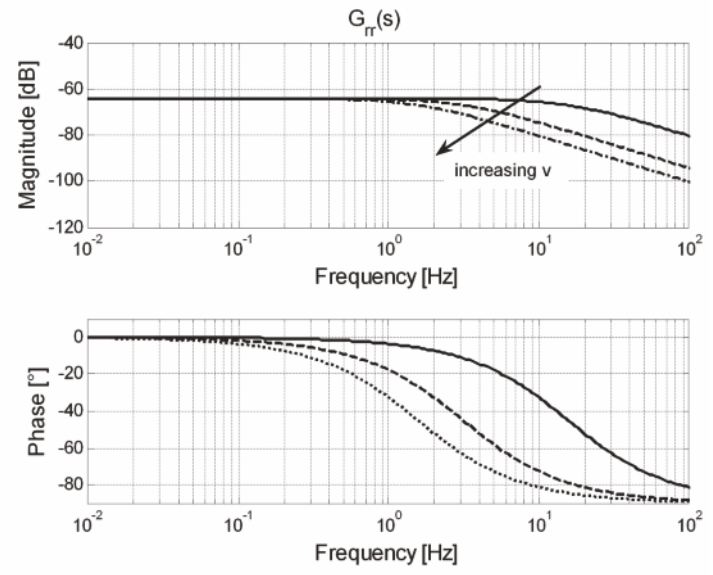

(b)

Figure 3.14 Magnitude and phase Bode plots of the frequency responses associated with $G_{\omega_f-\omega_r}(s)$ (a) and $G_{rr}(s)$ (b) for different vehicle speed values: $\overline{v} = 25$ m/s (*solid line*), $\overline{v} = 15$ m/s (*dashed line*) and $\overline{v} = 5$ m/s (*dash-dotted line*)

a simple and fixed structure PID controller has been designed to regulate the relative slip at the rear wheel.

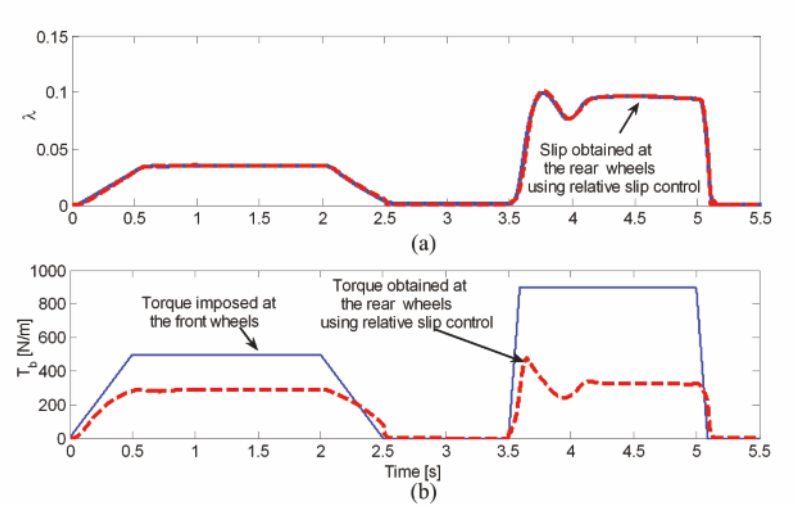

Figure 3.15 Plot of the wheel slip (a) and braking torque (b) in two braking manoeuvres with no control on the front wheel (dry asphalt and initial speed $v_0 = 100$ km/h)

Figures 3.15(a) and 3.15(b) show the rear wheel slip behaviour when the front wheel is in open-loop (the braking torque is imposed by the driver), and the rear wheel is controller using the relative slip as controlled variable, showing a good dynamic behaviour.

Finally, Figures 3.16(a) and 3.16(b) show the closed-loop behaviour of the wheel slip when a closed-loop slip controller (a simple PID controller of the type discussed in Section 3.4) acts on the front wheels and the rear wheels are regulated *via* relative slip control. In this case, when all the four wheels are controlled at the same time, the effects of dynamic coupling are more significant. However, the proposed control approach allows us to achieve a very good closed-loop performance with a SISO approach and two linear and fixed structure controllers.

3.8.3 Wheel Slip Control on Curves

Up to now we have always considered the wheel slip control problem under the assumption of negligible tyre sideslip angles, that is when the tyre–road contact forces are dominated by the longitudinal component.

When braking on a curve with non-negligible tyre sideslip angles, instead, one has to handle the trade-off between longitudinal and lateral forces (see

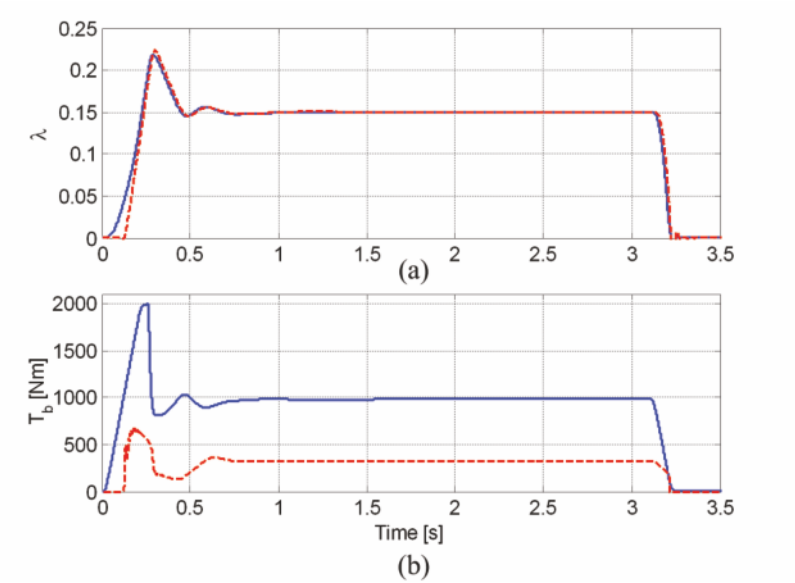

Figure 3.16 Plot of the wheel slip (a) and braking torque (b) in a hard braking manoeuvre on dry asphalt with front wheel slip control and rear wheels relative slip control. Front wheels (*solid line*) and rear wheel (*dashed line*)

Figures 2.2(a) and 2.2(b)). When on a curve, in fact, the largest amount of longitudinal force for transferring the braking torque to the ground is limited by the lateral force which is needed for negotiating the curve.

Thus, if the braking occurs in a curve manoeuvre where the vehicle is not subject to stability problems, that is when the ESC controller is not active, a wheel slip controller can be used by adapting the longitudinal slip set-point value $\overline{\lambda}$ to the curve condition. In four-wheeled vehicles this can be done by letting the set-point be a function of the steering angle (a variable commonly measured on all cars equipped with ESC systems), whereas in two-wheeled vehicles the set-point should be adapted as a function of the roll angle (see, *e.g.*, [108] and the references therein for a more detailed discussion on this topic). Besides the set-point adaptation, then, a wheel slip controller of the type discussed in this book is needed to handle the braking manoeuvre.

In the case of stability problems, instead, which in general occur when large values of the vehicle sideslip angle (*i.e.*, the angle between the chassis longitudinal axis and the velocity vector of the centre of mass) are reached, the ESC controller is activated. Some modern ESC controllers have a supervisory control logic that translates the yawing moment needed to recover stability into different wheel slip set-points commanded to each wheel and that are tracked by means of a slip controller of the type discussed in this book.

Other ESC controllers, instead, do not have this supervisory unit and directly act on the brakes to achieve the desired yawing moment, thus overriding the wheel slip control loop.

3.9 Summary

This chapter showed how to design braking controllers based on actuators with continuous dynamics.

Specifically, we first highlighted the advantages of controlling the wheel slip rather than the wheel deceleration, and discussed how to solve the slip control problem employing a linearised model of the single-corner dynamics. The tuning phase of different simple linear controllers was analysed in detail, providing the tuning rules to ensure closed-loop stability.

Further, the need for an activation and deactivation logic was motivated and a possible solution was outlined.

Finally, an analysis of the wheel slip control problem based on the double-corner model was presented, and its closed-loop stability properties were analysed.

Further, a control strategy based on the idea of interlocking the rear wheels with the front ones was presented, which imposes the same wheel slip behaviour on both axles and which is particularly interesting for vehicles presenting a large load transfer during braking.

Note finally that the stability proof carried out in Proposition 3.1 for the slip controller applied to the double-corner model could be extended to show that the stability of the equilibrium of the closed-loop system is indeed global and not only local. To do this, however, advanced concepts of nonlinear analysis are needed, which we believe go beyond the scope of this book and do not add crucial information to the specific problem. The interested reader can find the full proof in [115], together with some references to the related theoretical tools.